Plastic dynamics of the $Al_{0.5}CoCrCuFeNi$ high entropy alloy at cryogenic temperatures: Jerky flow, stair-like fluctuation, scaling behavior, and non-chaotic state

Xiaoxiang Guo, Xie Xie, Jingli Ren, Marina Laktionova, Elena Tabachnikova, Liping Yu, Wing-Sum Cheung, Karin A. Dahmen, and Peter K. Liaw

Citation: Appl. Phys. Lett. **111**, 251905 (2017); doi: 10.1063/1.5004241
View online: https://doi.org/10.1063/1.5004241
View Table of Contents: http://aip.scitation.org/toc/apl/111/25
Published by the American Institute of Physics

Plastic dynamics of the $Al_{0.5}CoCrCuFeNi$ high entropy alloy at cryogenic temperatures: Jerky flow, stair-like fluctuation, scaling behavior, and non-chaotic state

Xiaoxiang Guo,[1] Xie Xie,[2] Jingli Ren,[1,3,a)] Marina Laktionova,[4] Elena Tabachnikova,[4] Liping Yu,[1] Wing-Sum Cheung,[5] Karin A. Dahmen,[6] and Peter K. Liaw[2,a)]
[1]*School of Mathematics and Statistics, Zhengzhou University, Zhengzhou 450001, China*
[2]*Department of Materials Science and Engineering, The University of Tennessee, Knoxville, Tennessee 37996, USA*
[3]*State Key Laboratory of Nonlinear Mechanics, Institute of Mechanics, Chinese Academy of Science, Beijing 100190, China*
[4]*B.I. Verkin Institute for Low Temperature Physics and Engineering, National Academy of Sciences of Ukraine, Kharkiv 61103, Ukraine*
[5]*Department of Mathematics, The University of Hong Kong, Pokfulam, Hong Kong*
[6]*Department of Physics, University of Illinois at Urbana-Champaign, Urbana, Illinois 61801, USA*

(Received 12 September 2017; accepted 2 December 2017; published online 19 December 2017)

This study investigates the plastic behavior of the $Al_{0.5}CoCrCuFeNi$ high-entropy alloy at cryogenic temperatures. The samples are uniaxially compressed at 4.2 K, 7.5 K, and 9 K. A jerky evolution of stress and stair-like fluctuation of strain are observed during plastic deformation. A scaling relationship is detected between the released elastic energy and strain-jump sizes. Furthermore, the dynamical evolution of serrations is characterized by the largest Lyapunov exponent. The largest Lyapunov exponents of the serrations at the three temperatures are all negative, which indicates that the dynamical regime is non-chaotic. This trend reflects an ordered slip process, and this ordered slip process exhibits a more disordered slip process, as the temperature decreases from 9 K to 4.2 K or 7.5 K. *Published by AIP Publishing.* https://doi.org/10.1063/1.5004241

High-entropy alloys (HEAs) are new solid-solution alloys that contain five or more principal elements in equimolar or near-equimolar ratios and tend to have simple face-centered cubic (FCC), body-centered cubic (BCC), and hexagonal-closed-packed (HCP) structures.[1–4] It has been reported that HEAs exhibit many attractive properties, such as good ductility, high hardness, strong oxidation resistance, wonderful corrosion resistance, superior resistance to temper softening, super wear resistance, strong fatigue, and fracture resistance.[5–23] These remarkable properties make HEAs suitable advanced structural materials for many industries, including aerospace and ocean engineering.

For applications and basic materials sciences, it is important to investigate the performance of HEAs in different environments. The mechanical properties of HEAs are usually tested at different temperatures or strain rates, and in certain parameter regimes, serration behavior is found.[2] Serrations can be defined as a saw-like appearance of the stress-strain curves, a row of sharp or tooth-like jumps in stress or strain. One or two large and a number of smaller serrations were found on stress-strain curves during the plastic deformation at the temperature of 77 K for AlCoCrFeNi HEA.[24] Zhang *et al.* conclude that at lower temperatures, the serrations are more visible than at higher temperatures, and the serrations at a strain rate of $10^{-3}\,s^{-1}$ seem to be greater than those at a strain rate of $10^{-1}\,s^{-1}$ for the $Al_xCoCrCuFeNi$ HEAs under compression.[3] Carroll *et al.* propose a model that predicts the statistics of the serrations and identify the serrations as types-A, B, and C Portevin-Le Chatelier (PLC)-bands as the temperature varies from 275 °C to 700 °C for the CoCrFeMnNi HEA.[25]

Most of the published serrations stem from experiments at room temperature or elevated temperatures. Here, we study serrations at cryogenic temperatures where the deformation mechanisms may be different. Antonaglia *et al.*[26] found that the largest stress drops of serrations decrease as the temperature increases from 7 K to 9 K for the $Al_{0.5}CoCrCuFeNi$ HEA. A more detailed understanding of the serrated flow at these temperatures has been missing so far. In this paper, we investigate the plastic dynamics of the $Al_{0.5}CoCrCuFeNi$ HEA for cryogenic temperatures ranging from 4.2 K to 9 K. Jerky flows (serrated flows) and stair-like fluctuations are found during the evolution of stress and strain, respectively. The complex information of plastic deformation is revealed by statistical and dynamical analysis and modeling.

The samples, an $Al_{0.5}CoCrCuFeNi$ HEA, are fabricated by arc-melting the mixtures of constituent metals (Al, Cu, Cr, Co, Fe, and Ni) with purity higher than 99.9 weight percent (wt. %) in a Ti-gettered high-purity argon atmosphere. The process of melting and solidification is repeated at least five times to obtain chemical homogeneity. Then, the molten alloy is drop-cast into a water-cooled copper mold to form cylindrical rods with a diameter of 2 mm and a length of 50 mm. The specimens for compression tests are prepared by cutting the rod into 4 mm pieces in length. Both compression ends are polished to be parallel. The specimens are uniaxially compressed at a strain rate of 4×10^{-4}/s in a liquid helium environment, which are 4.2 K, 7.5 K, and 9 K in the present study by cooling the specimens with the helium steam. Loading of the

a)Authors to whom correspondence should be addressed: renjl@zzu.edu.cn and pliaw@utk.edu

specimens is terminated when deformation was ~20%–30% in the whole temperature range studied.

Stress and strain signals are obtained from the uniaxial compression tests. Figure 1 shows the strain-time, stress-time, and stress-strain curves at 4.2 K, 7.5 K, and 9 K, respectively. To clearly observe the fluctuations of strain and stress signals, we magnify the curves in Fig. 1. The magnified strain-time, stress-time, and stress-strain curves at 4.2 K are shown in Fig. 2 as an example.

For the strain-time curve, we find that it has stair-like fluctuations, see Fig. 2(a). By taking a close look, small fluctuations are detected on the horizontal direction, see a(i) → b(i) in the *i*th large serration as an example. It means that the $Al_{0.5}CoCrCuFeNi$ HEA undergoes small deformation with an elastic nature, and the elastic energy is stored during this stage. On the vertical direction of the stair-like structure,

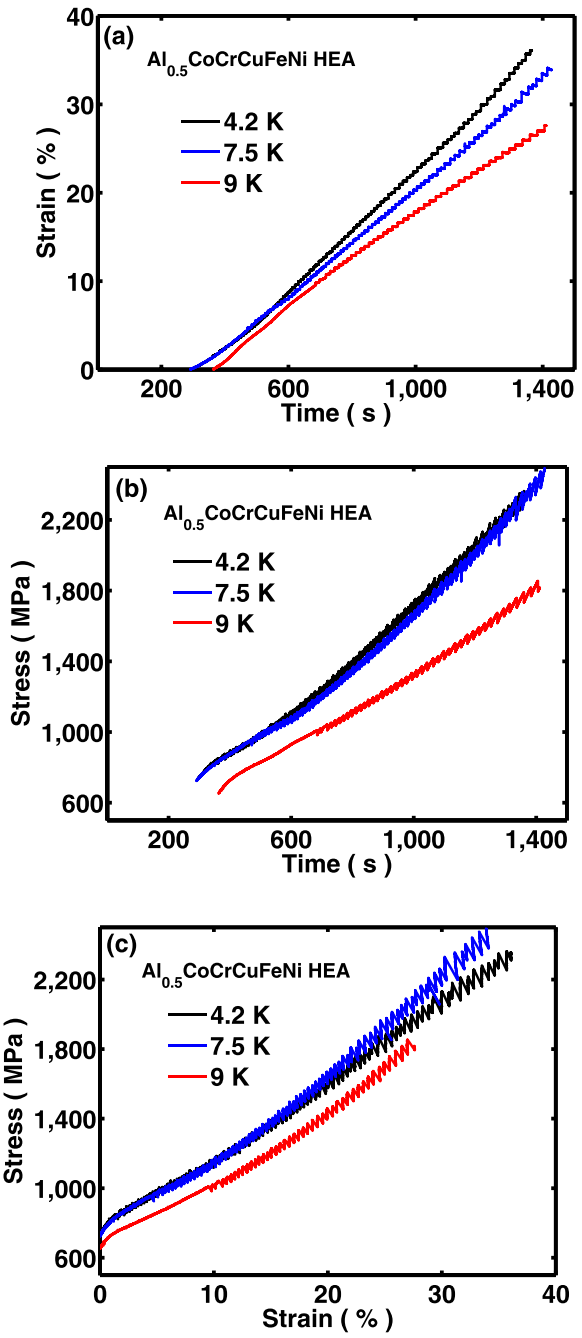

FIG. 1. Strain-time, stress-time, and stress-strain curves at 4.2 K, 7.5 K, and 9 K.

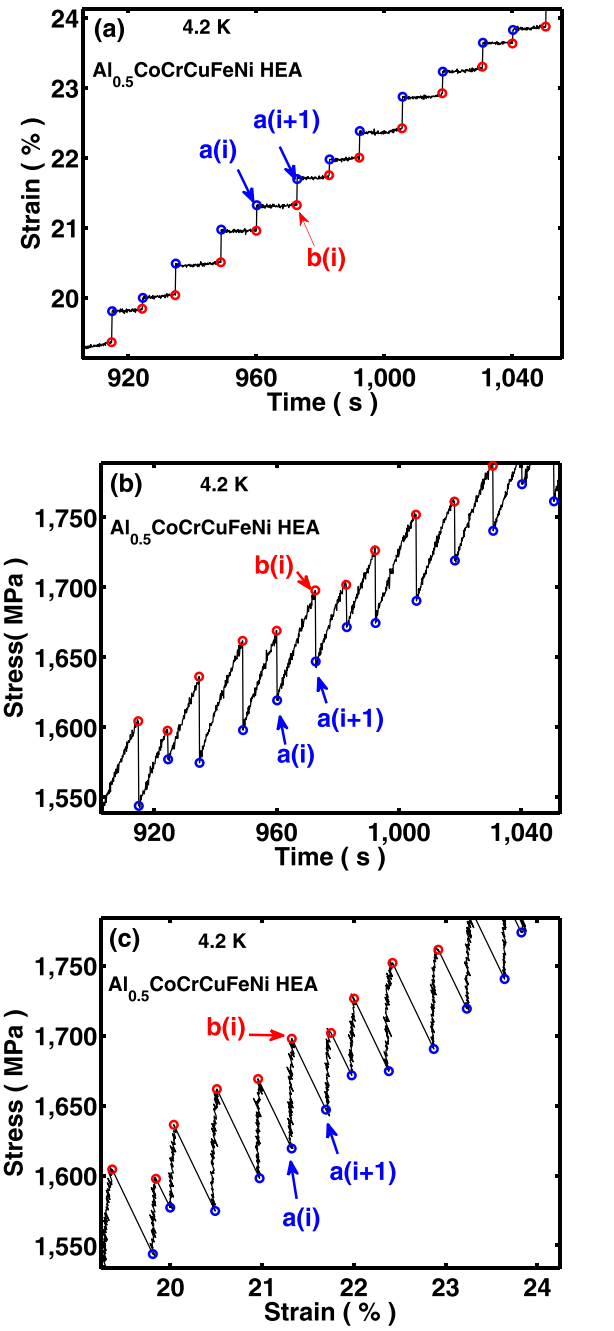

FIG. 2. The amplified strain-time, stress-time, and stress-strain curves at 4.2 K.

b(i) → a(i + 1), the suddenly increasing deformation is a plastic event that releases some of the stored elastic energy. So, there are discontinuities in the elastic-energy storage and release during the deformation from a(i) to a(i + 1).

Projecting the stair-like fluctuation of strain on the evolution of stress, we obtain the corresponding serrated flow, see Fig. 2(c). As is known, the stress fluctuations in the stress-strain curve are accompanied by changes in the elastic energy in the solid. Hence, it is a useful approach to investigate serration behavior by analyzing the changes in the elastic energy. The unit of stress is MPa = $N/m^2 = J/m^3$. The unit of strain is m/m as the strain signal is recorded by the variation of the length of the material, divided by the length of the sample. From a(i) to b(i), we denote the stress increase with $S_1(i)$ [MPa] and the strain change with $d_1(i)$. During this time, the

elastic energy is accumulated, i.e., the elastic energy accumulates when the material undergoes small deformation, denoting the average accumulated energy as

$$E_{ac}(i) = |S_1(i) \times d_1(i) \times V|/2, \tag{1}$$

where V is the volume of the sample. From b(i) to a(i + 1), the strain suddenly increases, the stress sharply decreases, and the accumulated elastic energy is released during this process. The stress decreases by $S_2(i)$ [MPa], the corresponding strain change is $d_2(i)$, and the released energy is

$$E_{re}(i) = |S_2(i) \times d_2(i) \times V|/2. \tag{2}$$

Figure 3(a) briefly shows the calculation of the accumulated elastic energy and released elastic energy. The material exhibits plastic deformation under compression, and strain increases, corresponding to the stress decrease. Then, we consider the stress drop, S_2, which should be a function of the corresponding strain-jump size, d_2, i.e., $S_2 = S_2(d_2)$. With Eq. (2), we calculate the released energy and strain variation, respectively, and plot the power-law fit of the relation, see Fig. 3(b). Then, we find that E_{re} satisfies the scaling behavior, $E_{re} \sim d_2^j$, see Table I for the values of j at different temperatures. It can be seen that the values of j are approximately equal to 2, as is to be expected from elasticity theory. In fact, according to the generalized Hooke's law, S_2 and $d_2(i)$ should satisfy

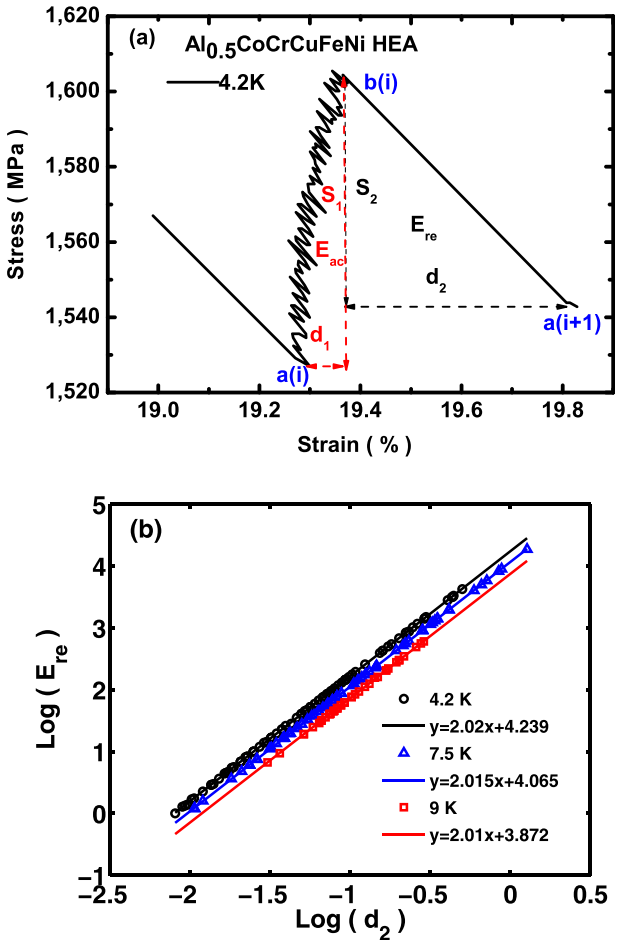

FIG. 3. (a) Illustration of the stress increase, S_1, the stress drop, S_2, the strain changes, d_1, and d_2, the accumulated energy, E_{ac}, and the released energy, E_{re}, on a large serration. (b) Power-law fit of the relation between the strain variation, d_2, and released energy, E_{re}, at 4.2 K, 7.5 K, and 9 K, respectively.

$S_2 = k \times d_2$, where k is the elastic coefficient. Recalling the definition of the released energy, we have the formula of $E_{re} \sim d_2^2$. Our experimental results are consistent with this prediction.

To extract more complex underlying information, we use tools from the chaotic time-series analysis to investigate the stress signal and characterize the dynamic behavior of serrations.

The evolution of stress is determined by the microstructure, slip form of slip bands, and other properties. Thus, the complex information about those properties is covered by this stress-evolution process. The property of the original system can be obtained through analyzing the evolution of the stress. According to the embedding dimension theorem developed by Takens *et al.*,[27,28] a time series can be embedded into a high dimensional space by the delay-coordinate technique. This high dimensional space is known as the reconstructed phase space, and the trajectory in the new phase space is diffeomorphic to the track in the original system.

Let a time series, $x_1, x_2, x_3, \ldots, x_N$, be embedded into an m-dimensional phase space by delay vectors. In the reconstructed phase space, a point is given as

$$\begin{aligned} Y(t) &= (x_t, x_{t+\tau}, x_{t+2\tau}, \ldots, x_{t+(m-1)\tau}), \\ t &= 1, 2, \ldots, N - (m-1)\tau, \end{aligned} \tag{3}$$

where m is the embedding dimension, τ is the time delay, m and τ are the positive integers. To completely illustrate the attractor in its space, the choice of the time delay, τ, and embedding dimension, m, should be chosen appropriately. If τ is too small, x_τ and $x_{t+\tau}$ cannot be separated; and if τ is too large, some evolution information will be lost, i.e., x_τ and $x_{t+\tau}$ will be less correlated. The new space cannot accurately reflect the evolution rules about the attractor. If m is too small, the attractor cannot be completely expanded, and a large m will increase the computational work.

In this paper, the time delay is calculated by the mutual information method.[29] The mutual information between the times, t and $t + \tau$, is defined as

$$I(X;\tau) = \sum_{t=1}^{N-\tau} P(x_t, x_{t+\tau}) log_2 \left[\frac{P(x_t, x_{t+\tau})}{P(x_t)P(x_{t+\tau})} \right], \tag{4}$$

where X is a time series, $\{x_t\}$, $P(x_t), P(x_{t+\tau})$, and $P(x_t, x_{t+\tau})$ are the probabilities and joint probability of x_t and $x_{t+\tau}$ appearing in the time series, respectively. For a given time series, $\{x_t\}$, the mutual information, I, is only dependent on τ, i.e., $I(\tau)$. $I(\tau)$ reflects the correlation between $\{x_t\}$ and $\{x_{t+\tau}\}$. When $I(\tau)$ first reaches its local minimum value, the corresponding time delay, τ_0, is the optimal time delay to reconstruct the phase space.[29] Denote the acquisition time of the stress signal by h, then the true time corresponding to τ_0 is $\tau_t = \tau_0 \times h$.

For example, Fig. 4(a) shows the mutual information, $I(\tau)$, as a function of time delay, τ, and the suitable time

TABLE I. The values of j at 4.2 K, 7.5 K, and 9 K.

Parameter \ Temperature	4.2 K	7.5 K	9 K
j	2.020	2.015	2.010

delay, $\tau_0 = 9$, at 7.5 K. The values of τ_0, h, and τ_t at different temperatures are shown in Table II. Then, we focus on the mean time intervals of large serrations, t_M, and the frequency of the large avalanches, $v = 1/t_M$. Comparing the values of t_M and v to τ_0 at different temperatures (see Table II), we find that τ_t has an opposite change tendency with t_M but the same change tendency with v. So, τ_t may be positively related to v. Furthermore, the size of the resulting time delay, τ_0, reflects the degree of correlations among the slip bands, during the stress evolution. The smaller the optimal time delay, the stronger the correlation that the slip bands have.

The embedding dimension is computed by the Cao method.[30] For a point

$$Y_i(t) = (x_t, x_{t+\tau}, x_{t+2\tau}, \ldots, x_{t+(m-1)\tau}),$$

in the m-dimensional space, denotes its nearest neighbor point (in the sense of Euclid Norm) by

$$Y_i^*(t) = (x_t^*, x_{t+\tau}^*, x_{t+2\tau}^*, \ldots, x_{t+(m-1)\tau}^*).$$

The distance between these two points is $d_i^m = ||Y_i(t) - Y_i^*(t)||_{(m)}$. While the embedding dimension increases to $m+1$, the distance becomes $d_i^{m+1} = ||Y_i\ (t) - Y_i^*(t)||_{(m+1)}$. Let $a(i,m) = \frac{d_i^m}{d_i^{m+1}}$, where d_i^m is the distance in m dimensional space, and d_i^{m+1} is the distance in $m+1$ dimensional space. $a(i,\ m)$ reflects the change of distance with increasing the dimension of phase space. Then, taking the average over all points in the phase space, we have $A(m) = \frac{1}{N-(m-1)\tau} \sum_{i=1}^{N-(m-1)\tau} a(i,m)$ and $A^*(m) = \frac{1}{N-(m-1)\tau} \sum_{i=1}^{N-(m-1)\tau} |x_{i+m\tau} - x_{i+m\tau}^*|$. The change of the average distance is defined as $E_1(m) = \frac{A(m)}{A(m-1)}$ and $E_2(m) = \frac{A^*(m)}{A^*(m-1)}$, which are functions of the embedding dimension, m. We obtain the embedding dimension, m_0, when $E_1(m)$ tends to be steady and $E_2(m)$ approaches 1. Figure 4(b) shows $E_1(m)$ and $E_2(m)$ as a function of the embedding dimension, m, and the optimal embedding dimension, $m_0 = 12$, is obtained at 7.5 K. The embedding dimension, m, is the dimension of the reconstructed phase space. The appropriate embedding dimensions at 4.2 K and 9 K are shown in Table II.

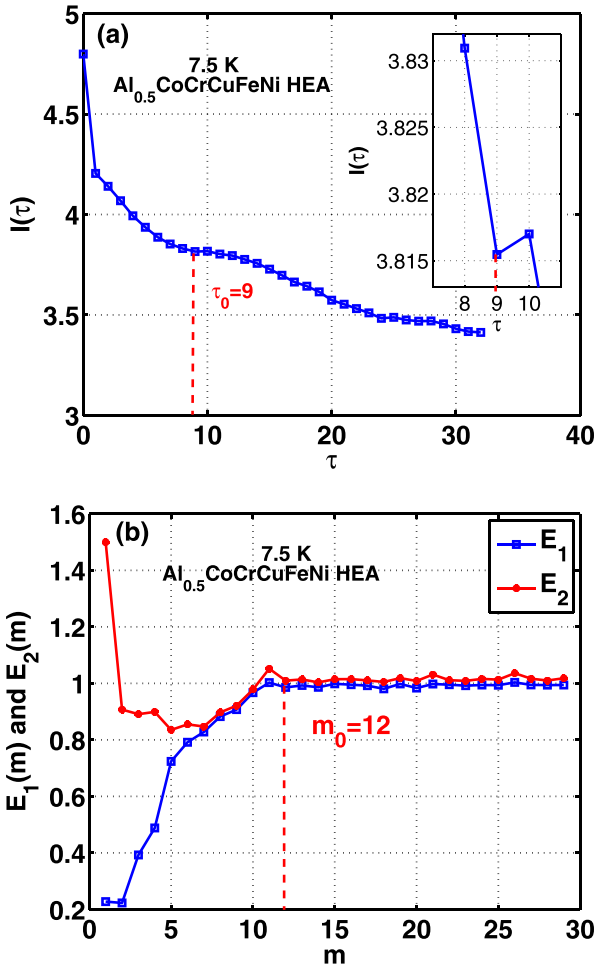

FIG. 4. (a) The mutual information, I(τ), as a function of the time delay, τ, at 7.5 K. The inset shows the magnification near $\tau = 9$. (b) $E_1(m)$ and $E_2(m)$ as a function of the embedding dimension, m, at 7.5 K.

TABLE II. The optimal time delay, τ_0, acquisition time, h, true time corresponding to τ_0, τ_t, mean time interval of large serrations, t_M, frequency of large avalanches, v, optimal embedding dimension, m_0, and largest Lyapunov exponent, λ, at 4.2 K, 7.5 K, and 9 K.

Parameter \ Temperature	4.2 K	7.5 K	9 K
τ_0	26	9	9
h (s)	0.145	0.150	0.130
τ_t (s)	3.77	1.35	1.17
t_M (s)	5.2834	5.6479	8.4823
v (Hz)	0.1893	0.1771	0.1179
m_0	6	12	16
λ	−7.3420e-4	−4.4502e-4	−0.0197

After reconstructing the phase space, we calculate the largest Lyapunov exponent (LLE) of the stress signal, which quantifies the rate of divergence of the trajectories in the phase space. It reflects how the orbit moves together or apart with the evolution of the stress signal. A positive LLE would suggest that the dynamic follows chaotic behavior, while a negative LLE indicates a stable state. Here, we use Wolf's method to calculate the largest Lyapunov exponent.[31–35] We take an initial point, $Y\ (t_0)$, and its nearest neighbor point, $Y_0^*(t_0)$, in the reconstructed phase space. Then, the distance between these two points is $L_0 = |Y(t_0) - Y_0^*(t_0)|$. Tracking the evolution of these two points till time, t_1, the two points evolve to be $Y(t_1)$ and $Y_0^*(t_1)$, and the distance, L_0, changes to be $L_0' = |Y(t_1) - Y_0^*(t_1)| > \omega$, where ω is a given constant, which is slightly larger than the minimum distance of each two points in the reconstructed phase space. At the time, t_1, $Y_0^*(t_1)$ may not be the nearest neighbor point of $Y(t_1)$. Thus, we find another point, $Y_1^*(t_1)$, which is the nearest neighbor point to $Y(t_1)$. The distance between these two points is $L_1 = |Y(t_1) - Y_1^*(t_1)|$, and we set the angle between L_0' and L_1 as small as possible to ensure that the influence on orbit evolution is small, when we choose the nearest neighbor point. Then, tracking the evolution to obtain L_1' and repeating the above process until the end of the time series, we obtain the number of these iterations, K. Here, we have

$$L_i = |Y(t_i) - Y_i^*(t_i)|, \quad L_i' = |Y(t_{i+1}) - Y_i^*(t_{i+1})|, \quad i = 0, 1, \ldots, K. \tag{5}$$

The largest Lyapunov exponent is

$$\lambda = \frac{1}{t_K - t_0} \sum_{i=0}^{K} ln \frac{L_i'}{L_i}. \quad (6)$$

A positive value of λ reflects that the dynamical behavior of the serrated flow is chaotic, the orbits in the phase space move apart, and the evolution of orbits is long-range unpredictable. A chaotic system is sensitive to the initial point, and the system is unstable. Projecting a chaotic system onto a one-dimensional stress signal, the evolution of the stress signal presents the diffeomorphism to the development of orbits in a chaotic system. Hence, the serrations under a chaotic regime appear disordered because the orbit in the chaotic system spreads apart.

A negative value of λ indicates that the dynamic behavior is stable, and the trajectories in the phase space move together. The serrations in a stable dynamical regime appear ordered as the orbit in the stable system is convergent. The appearance of slip bands can be reflected by the evolution of the serrated flow. Thus, the slip dynamics of plastic deformation under the stable regime is ordered.

The values of the largest Lyapunov exponents at different temperatures are shown in Table II. The values are negative, but the moduli of the values at 4.2 K and 7.5 K are very small, apparently approaching zero. From these values, we can say that the dynamic regime of the stress evolution is stable, and the slip form of plastic deformation is ordered at 9 K. Remarkably at 4.2 K and 7.5 K, the stability of the system weakens, and the slip dynamics appears to tend towards being disordered.

In summary, serrations and stair-like fluctuations are found in the evolution of stress and strain, respectively. A scaling relationship between the released elastic energy and strain-jump sizes is detected by statistical analysis and modeling. The dynamical regimes of the serration behavior at 4.2 K, 7.5 K, and 9 K are characterized by the largest Lyapunov exponents (negative), which shows that the dynamics are stable, and the slip process of the plastic deformation is ordered. Remarkably, this stability weakens and the slip process has a trend towards being disordered when the temperature changes from 9 K to 7.5 K or 4.2 K.

J. L. Ren is very grateful for the financial support from the Natural Science Foundation of China (11771407), the Plan for Scientific Innovation Talent of Henan Province (164200510011), the Innovative Research Team of Science and Technology in the Henan Province (17IRTSTHN007), the National Key Research and Development Program of China (2017YFB0702504), and the Opening fund of the State Key Laboratory of Nonlinear Mechanics (LNM201710). K. A. Dahmen and P. K. Liaw would like to acknowledge the Department of Energy (DOE), Office of Fossil Energy, National Energy Technology Laboratory (DE-FE-0008855, DE-FE-0024054, and DE-FE-0011194), with Mr. V. Cedro, Mr. R. Dunst, Dr. P. Rawls, and Dr. J. Mullen as program managers. P. K. Liaw very much appreciates the support of the U.S. Army Research Office project (W911NF-13-1-0438) with the program managers, Dr. M. P. Bakas and Dr. D. M. Stepp. P. K. Liaw thanks the support from the National Science Foundation (DMR-1611180) with the program director, Dr. D. Farkas.

[1]J. W. Yeh, S. K. Chen, S. J. Lin, J. Y. Gan, T. S. Chin, T. T. Shun, C. H. Tsau, and S. Y. Chang, Adv. Eng. Mater. **6**, 299–303 (2004).
[2]Y. Zhang, J. P. Liu, S. Y. Chen, X. Xie, P. K. Liaw, K. A. Dahmen, J. W. Qiao, and Y. L. Wang, Prog. Mater. Sci. **90**, 358–460 (2017).
[3]Y. Zhang, T. T. Zuo, Z. Tang, M. C. Gao, K. A. Dahmen, P. K. Liaw, and Z. P. Lu, Prog. Mater. Sci. **61**, 1–93 (2014).
[4]K. M. Youssef, A. J. Zaddach, C. N. Niu, D. L. Irving, and C. C. Koch, Mater. Res. Lett. **3**, 95–99 (2015).
[5]Z. W. Wang, I. Baker, Z. H. Cai, S. Chen, J. D. Poplawsky, and W. Guo, Acta Mater. **120**, 228–239 (2016).
[6]B. Gludovatz, A. Hohenwarter, D. Catoor, E. H. Chang, E. P. George, and R. O. Ritchie, Science **345**, 1153–1158 (2014).
[7]L. J. Santodonato, Y. Zhang, M. Feygenson, C. M. Parish, M. C. Gao, R. J. K. Weber, J. C. Neuefeind, Z. Tang, and P. K. Liaw, Nat. Commun. **6**, 5964 (2015).
[8]Y. Zhang, Y. J. Zhou, J. P. Lin, G. L. Chen, and P. K. Liaw, Adv. Eng. Mater. **10**, 534–538 (2008).
[9]T. Borkar, B. Gwalani, D. Choudhuri, C. V. Mikler, C. J. Yannetta, X. Chen, R. V. Ramanujan, M. J. Styles, M. A. Gibson, and R. Banerjee, Acta Mater. **116**, 63–76 (2016).
[10]N. A. P. Kiran, C. Li, K. J. Leonard, H. Bei, and S. J. Zinkle, Acta Mater. **113**, 230–244 (2016).
[11]F. Otto, A. Dlouhy, K. G. Pradeep, M. Kubenova, D. Raabe, G. Eggeler, and E. P. George, Acta Mater. **112**, 40–52 (2016).
[12]Z. Q. Fu, W. P. Chen, H. M. Wen, D. L. Zhang, Z. Chen, B. L. Zheng, Y. Z. Zhou, and E. J. Lavernia, Acta Mater. **107**, 59–71 (2016).
[13]S. Maiti and W. Steurer, Acta Mater. **106**, 87–97 (2016).
[14]O. N. Senkov, G. B. Wilks, D. B. Miracle, C. P. Chuang, and P. K. Liaw, Intermetallics **18**, 1758–1765 (2010).
[15]O. N. Senkov, G. B. Wilks, J. M. Scott, and D. B. Miracle, Intermetallics **19**, 698–706 (2011).
[16]O. N. Senkov, J. M. Scott, S. V. Senkova, D. B. Miracle, and C. F. Woodward, J. Alloys Compd. **509**, 6043–6048 (2011).
[17]C. J. Tong, M. R. Chen, S. K. Chen, J. W. Yeh, T. T. Shun, S. J. Lin, and S. Y. Chang, Metall. Mater. Trans. **36A**, 1263–1271 (2005).
[18]O. N. Senkov, S. V. Senkova, D. B. Miracle, and C. Woodward, Mater. Sci. Eng. A **565**, 51–62 (2013).
[19]Y. F. Kao, T. J. Chen, S. K. Chen, and J. W. Yeh, J. Alloys Compd. **488**, 57–64 (2009).
[20]S. C. Middleburgh, D. M. King, G. R. Lumpkin, M. Cortie, and L. Edwards, J. Alloys Compd. **599**, 179–182 (2014).
[21]J. M. Wu, S. J. Lin, J. W. Yeh, S. K. Chen, Y. S. Huang, and H. C. Chen, Wear **261**, 513–519 (2006).
[22]M. H. Chuang, M. H. Tsai, W. R. Wang, S. J. Lin, and J. W. Yeh, Acta Mater. **59**, 6308–6317 (2011).
[23]M. A. Hemphill, T. Yuan, G. Y. Wang, J. W. Yeh, C. W. Tsai, A. Chuang, and P. K. Liaw, Acta Mater. **60**, 5723–5734 (2012).
[24]J. W. Qiao, S. G. Ma, E. W. Huang, C. P. Chuang, P. K. Liaw, and Y. Zhang, Mater. Sci. Forum **688**, 419–425 (2011).
[25]R. Carroll, C. Lee, C. W. Tsai, J. W. Yeh, J. Antonaglia, B. W. Brinkman, M. LeBlanc, X. Xie, S. Y. Chen, P. K. Liaw, and K. A. Dahmen, Sci. Rep. **5**, 16997 (2015).
[26]J. Antonaglia, X. Xie, K. A. Dahmen, Z. Tang, P. K. Liaw, J. W. Yeh, C. W. Tsai, J. W. Qiao, Y. Zhang, M. O. Laktionova, E. D. Tabachnikova, O. N. Senkov, M. C. Gao, and J. T. Uhl, JOM **66**, 2002–2008 (2014).
[27]F. Takens, Lect. Notes Math. **898**, 366–381 (1981).
[28]N. H. Nackard, J. P. Crutchfield, J. D. Farmer, and R. S. Shaw, Phys. Rev. Lett. **45**, 712–716 (1980).
[29]A. M. Fraser and H. L. Swinney, Phys. Rev. A **33**, 1134–1140 (1986).
[30]L. Cao, Physica D **110**, 43–50 (1997).
[31]A. Wolf, J. B. Swift, H. L. Swinney, and J. A. Vastano, Physica D **16**, 285–317 (1985).
[32]S. Y. Chen, L. P. Yu, J. L. Ren, X. Xie, X. P. Li, Y. Xu, G. F. Zhao, P. Z. Li, F. Q. Yang, Y. Ren, and P. K. Liaw, Sci. Rep. **6**, 29798 (2016).
[33]J. L. Ren, C. Chen, G. Wang, N. Matterm, and J. Eckert, AIP Adv. **1**, 032158 (2011).
[34]J. L. Ren, C. Chen, Z. Y. Liu, R. Li, and G. Wang, Phys. Rev. B **86**, 134303 (2012).
[35]C. Chen, J. L. Ren, G. Wang, K. A. Dahmen, and P. K. Liaw, Phys. Rev. E **92**, 012113 (2015).